Nanoscale Advances

ROYAL SOCIETY OF CHEMISTRY

PAPER

View Article Online
View Journal | View Issue

Cite this: *Nanoscale Adv.*, 2021, **3**, 6213

Magneto-mechanical treatment of human glioblastoma cells with engineered iron oxide powder microparticles for triggering apoptosis†

C. Thébault, [ab] M. Marmiesse,[a] C. Naud, [a] K. Pernet-Gallay, [c] E. Billiet,[a] H. Joisten, [ad] B. Dieny, [a] M. Carrière, [*b] Y. Hou [*b] and R. Morel [*a]

In nanomedicine, treatments based on physical mechanisms are more and more investigated and are promising alternatives for challenging tumor therapy. One of these approaches, called magneto-mechanical treatment, consists in triggering cell death *via* the vibration of anisotropic magnetic particles, under a low frequency magnetic field. In this work, we introduce a new type of easily accessible magnetic microparticles (MMPs) and study the influence of their surface functionalization on their ability to induce such an effect, and its mechanism. We prepared anisotropic magnetite microparticles by liquid-phase ball milling of a magnetite powder. These particles are completely different from the often-used SPIONs: they are micron-size, ferromagnetic, with a closed-flux magnetic structure reminiscent of that of vortex particles. The magnetic particles were covered with a silica shell, and grafted with PEGylated ligands with various physicochemical properties. We investigated both bare and coated particles' *in vitro* cytotoxicity, and compared their efficiency to induce U87-MG human glioblastoma cell apoptosis under a low frequency rotating magnetic field (RMF). Our results indicated that (1) the magneto-mechanical treatment with bare MMPs induces a rapid decrease in cell viability whereas the effect is slower with PEGylated particles; (2) the number of apoptotic cells after magneto-mechanical treatment is higher with PEGylated particles; (3) a lower frequency of RMF (down to 2 Hz) favors the apoptosis. These results highlight a difference in the cell death mechanism according to the properties of particles used – the rapid cell death observed with the bare MMPs indicates a death pathway *via* necrosis, while PEGylated particles seem to favor apoptosis.

Received 21st June 2021
Accepted 21st September 2021

DOI: 10.1039/d1na00461a

rsc.li/nanoscale-advances

Introduction

Magnetic nanoparticles are widely studied and used for different biomedical and bioengineering applications, including hyperthermia, magnetic resonance imaging, drug delivery, and biosensing.[1] More recently, the use of magnetic microparticles (MMPs) for biomedical applications has attracted an increasing interest. One promising example is the destruction of cancer cells induced by low-frequency magneto-mechanical vibration of particles, by the application of an external magnetic field.[2,3] Such a research field opens perspectives for a new and effective therapeutic approach.[4] The interest in the modulation of the cell physiology using mechanical stimulation also stems from the recent recognition of the importance of mechanotransduction in the mechanisms associated with tumor progression, besides the classical molecular pathways governing cancer.[5]

From a material design point of view, the magnetic properties that are required for this application differ from those of the widely used superparamagnetic iron oxide nanoparticles (SPIONs).[6] First, their vibration must result in a mechanical stress sufficient to induce a response of the cell. Some examples show either the opening of mechanosensitive ion channels, for which a stress in the range of 1–10 kPa is required,[7] or damage to the cell membrane, for which a higher stress is required (10–15 kPa).[8] Other cell responses are reported in the review by Golovin *et al.*[9] The magnetic torque experienced by a particle under the application of an external magnetic field is proportional to its magnetization. With micron size particles, it can reach a few tens of fN m, which will locally generate stresses of a few tens of kPa.[10]

In addition to this size requirement, the particles should have a low magnetization remanence to avoid agglomeration caused by their magnetostatic interactions. They should also

[a]*Univ. Grenoble Alpes, CEA, CNRS, Spintec, 38000 Grenoble, France. E-mail: robert.morel@cea.fr*

[b]*Univ. Grenoble Alpes, CEA, CNRS, IRIG-SyMMES, 38000 Grenoble, France. E-mail: marie.carriere@cea.fr; yanxia.hou-broutin@cea.fr*

[c]*Univ. Grenoble Alpes, Inserm, U1216, CHU Grenoble Alpes, CEA, Grenoble Institut Neurosciences, Grenoble, France*

[d]*Univ. Grenoble Alpes, CEA, LETI, 38000 Grenoble, France*

† Electronic supplementary information (ESI) available. See DOI: 10.1039/d1na00461a

have good biocompatibility, *i.e.*, no intrinsic cell toxicity and good colloidal stability under physiological conditions. Finally, they should allow surface functionalization to enable specific interactions with the cells, for instance to ensure specific cell-targeting.

Most often these particles are thin discs with a diameter close to a micron and a thickness of a few tens of nanometers, whose magnetic properties result from appropriate choice of size, shape, and multilayered composition. The most commonly used structures are synthetic antiferromagnets with planar or perpendicular magnetizations, and vortex microparticles.[11] These particles are essentially made of ferromagnetic transition metals (Fe, Co, Ni), with other non-magnetic elements (Ru, B, Pt, Ta) to provide them the desired properties. They are produced by top-down approaches including lithography, etching and/or lift-off techniques, most often in a clean room facility. Consequently, the main disadvantage compared to SPIONs is the higher cost of fabrication, their low production yield, as well as their lack of biocompatibility.

To address these drawbacks and insure that the particles can be biocompatible, an alternative solution is to use easily accessible micron-size iron oxide particles. The SPIONs that are widely used for biomedical applications are in a size range of a few nanometer in diameter at which they are super-paramagnetic. The particles we discuss here are in the normal ferrimagnetic state. One important feature making them suitable for biomedical application is that they consist of magnetite grains with a closed-flux magnetic structure.[12,13] This contributes to the low magnetic remanence, which is one of the requirement to ensure good dispersion of the particles in solutions.[14]

It must however be kept in mind that the use of magnetic particles for biomedical applications involves many pitfalls, as evidenced by the difficulties encountered with SPIONs, notably in the development of particles for drug delivery and imaging. These difficulties have been described and discussed in many review papers to which the reader is referred.[15–17]

One example of below-expectation result is with drug delivery where, despite interesting results often obtained with SPIONs in *in vitro* experiment, the delivery efficiency with intravenous injection is as low as 0.7%. Many factors may contribute to this, among which is the fact that tumor targeting often relies on the enhanced permeability and retention (EPR) effect, which in some cases may not be as efficient as expected. Even if the targeting efficiency can be improved by specific surface functionalization, the protein-corona that rapidly covers the particles significantly modify their physico-chemical properties in an adverse way.[18,19] Micron-size magnetic particles differ from SPIONs regarding these two aspects. For one thing, they are not intended for targeted-delivery using the EPR effect (their diameter is above the reported endothelial gap size[20]) and their administration is done locally, at the tumor site, by injection.[4] Although reports of *in vivo* experiment are scarce, it appears that even many days after injection the particles remain mostly close to the injection site, meaning that they can be magnetically activated over long period.

The cell–particles interaction is also different according to the particle size. Small particles enter the cell *via* clathrin-mediated endocytosis, and cells can internalize thousands of SPIONs that accumulate in lysosomal cavities, where their decay can induce dysfunction.[21] Lysosome internalization is nevertheless not necessarily detrimental, as the magneto-mechanical stimulation of lysosome-entrapped SPIONs has been reported to induce cancer cell death, either by lysosomal membrane permeabilization[22–24] or by damaging the cytoskeleton.[25]

Regarding larger particles, caveolae-mediated internalization has been reported for latex spheres up to, but not larger than 500 nm.[26] Apart from the endocytosis mechanism, one observation is that, contrary to small particles, no delivery to the lysosomes is observed for the large ones. Internalization of magnetic particles and nanowires with length well above 1 μm has also been reported, although no mechanism for internalization has been identified.[27–29]

In this paper, we report on the development of a new type of magnetic microparticles, obtained *via* ball milling of magnetite powder, and their use for triggering apoptosis of cancer cells. Such a simpler manufacturing process allows the production of large quantities of particles in an easy way and at low cost. The average particle size and magnetic properties are optimized to be suitable for the destruction of cancer cells. In addition, to ensure their long-term stability in physiological conditions, the magnetic microparticles are covered by a silica shell. One advantage using silica as a coating material lies in its compatibility with various surface chemistry for the introduction of diverse surface properties such as charge and hydrophobicity.[30] It has been reported that surface charge and surface hydrophobicity are among the main influencing factors for cytotoxicity in addition to the material, size, shape, and composition of particles.[31] Herein, the silica shell is further functionalized with diverse poly(ethylene glycol) (PEG) ligands with different charge and length to study their effect on the efficiency for cell apoptosis induction. PEGylated coatings are highly biocompatible with excellent anti-fouling property and high steric hindrance to stabilize particles. They are often used to prolong vascular circulation of nanoparticles like SPIONs.[1] In this study, the effect of surface coating charge and thickness, duration and frequency of the applied magnetic field on their efficiency for apoptosis induction was investigated.

Results and discussion

Magnetic microparticle synthesis and optimization by ball milling

MMP were obtained by ball milling of magnetite powder. To characterize the size of these anisotropic particles, the Feret and MinFeret diameters were measured from SEM pictures of initial powder and after 1 h, 2 h, 4 h or 12 h of ball milling (some examples in Fig. 1a–c). Fig. 1d shows the size distribution of the initial powder compared to the size distribution of MMP after 4 h of ball milling.

When fitting the MMP size distribution using a lognormal law, after 1 h, 2 h, 4 h or 12 h of ball milling, the Mean Feret diameter of the initial powder that was measured at 3.2 μm

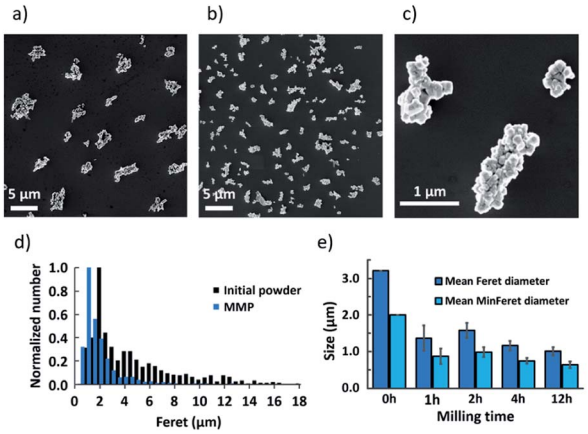

Fig. 1 SEM images of the initial powder (a) and particles after 4 h of ball milling (b and c). (d) Feret diameter distribution for the initial powder and for particles after 4 h of ball milling (MMP). (e) Mean Feret and Mean MinFeret diameters for the initial powder and after 1, 2, 4 and 12 h of ball milling, calculated from the lognormal size distribution fitting.

decreased to 1.4 µm, 1.6 µm, 1.2 µm and 1.0 µm, respectively (Fig. 1e). Accordingly, the Mean MinFeret diameter initially at 2.0 µm was reduced to 0.9 µm, 1.0 µm, 0.7 µm and 0.6 µm, respectively.

In particular, 4 h-ball milling process resulted in the formation of magnetite particles, composed of sintered smaller crystallites, with an average size close to one micron that is well suited for our purpose (Fig. 1b and c). Therefore, in this study, the particles obtained after 4 h of ball milling, which we hereafter denote MMP, were used for the further experiments. All these results confirm that ball milling is a very efficient, simple, rapid and cost-effective process for preparation of large quantities of anisotropic magnetite microparticles.

Characterization of the magnetic microparticles

First, bare MMP were characterized to obtain their XRD profile and magnetization curve. The XRD measurements with both initial powder and MMP matched with the expected $Fd\bar{3}m(227)$ space group for Fe_3O_4 (PDF 01-080-6402 (ref. 32)), with a slight peak deformation indicating a small structural inhomogeneity (Fig. 2a). On the other hand, no contribution from maghemite or other iron oxide phase could be identified before or after milling. The lattice parameters for the initial powder and for MMP were, respectively, $a = 8.392(5)$ Å and $a = 8.391(5)$ Å. These values are very close to the reported lattice parameter for bulk magnetite ($a = 8.3967(3)$ Å).[33] The crystallite sizes before and after milling were, respectively, 80 nm and 98 nm. Given the peak deformation, the difference is not significant.

The saturation mass magnetization of the MMP was measured at 83 A m^2 kg^{-1} (Fig. 2b). This is lower than the bulk value (92 A m^2 kg^{-1}),[34] but is typical for magnetite particles.[8] The remanent magnetization was 16 A m^2 kg^{-1}, and the coercivity 10.6 mT; both values are again typical for particles close to the single domain – multi domain critical size.[35] Afterwards, MMP were first covered by a silica shell and then functionalized with diverse PEG ligands following the procedures given in Fig. 3. The functionalized particles were characterized by measuring their zeta potential, which is related to their net surface charge. In this study, in order to evaluate the effect of surface coating charge and thickness on the magneto-mechanical treatment efficacy, different functionalization of the MMP were performed using diverse PEG with distinct terminal group (–OH, –NH_2, –COOH) and length (the detailed step-by-step functionalization of MMP is described hereafter in the Materials and methods section). To simplify notation, particles were labeled as detailed in Table 1.

The MMP have a negative zeta potential of −50 mV. After the formation of the silica shell, as expected, zeta potential of MMP@SiO_2 shifted to −36 mV. At the end, four different PEGs were grafted onto the magnetic particles, allowing to obtain PEGylated particles MMP@$PEG_{280}NH_2$, MMP@$PEG_{280}COOH$, MMP@$PEG_{150}OH$ and MMP@$PEG_{2000}OH$. The zeta potential of these particles were −10 mV, −38 mV, −24 mV and −22 mV, respectively (Table 2). These results show that the functionalized particles have differential surface charge and confirm the successful immobilization of PEG on the particles. It is generally admitted that a zeta potential above 30 mV or below −30 mV is indicative of good NP dispersion property, while small zeta potential values indicate a tendency to aggregation. In our case, as will be shown hereafter, the PEGylated particles show the best *in vitro* dispersion while bare particles, with the highest zeta potential, tend to aggregate in more complex milieu. Possible cause for the aggregation is either the magnetic

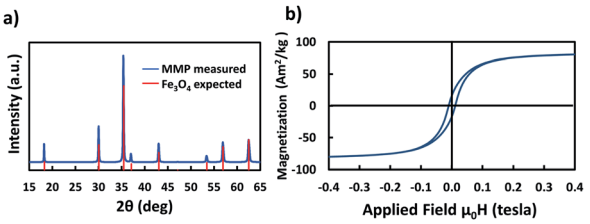

Fig. 2 (a) X-ray diffraction spectra and (b) magnetization curve of MMP obtained after 4 h of ball milling.

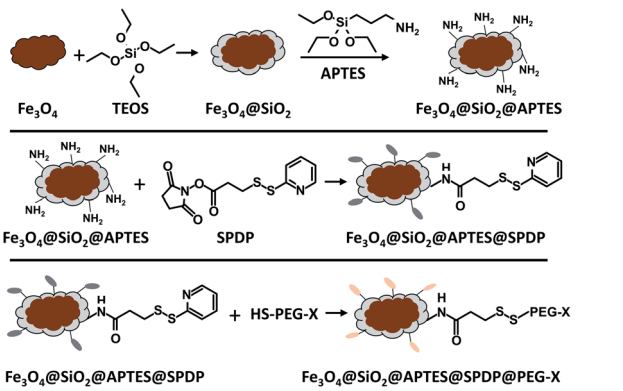

Fig. 3 Schematic illustration of the surface functionalization of magnetite particles.

Table 1 Notation of the different magnetic particles

Bare magnetite particles after 4 h of milling	MMP
Fe_3O_4@SiO_2	MMP@SiO_2
Fe_3O_4@SiO_2@APTES	MMP@APTES
Fe_3O_4@SiO_2@APTES@SPDP@$(CH_2)_{11}PEG_{280}NH_2$	MMP@$PEG_{280}NH_2$
Fe_3O_4@SiO_2@APTES@SPDP@$(CH_2)_{11}PEG_{280}CH_2COOH$	MMP@$PEG_{280}COOH$
Fe_3O_4@SiO_2@APTES@SPDP@$(CH_2)_6PEG_{150}OH$	MMP@$PEG_{150}OH$
Fe_3O_4@SiO_2@APTES@SPDP@$PEG_{2000}OH$	MMP@$PEG_{2000}OH$

Table 2 Zeta potential of magnetic microparticles with different surface coatings

	Zeta potential (mV)
MMP	-50.0 ± 2.3
MMP@SiO_2	-36.2 ± 0.9
MMP@$PEG_{280}NH_2$	-10.1 ± 1.5
MMP@$PEG_{280}COOH$	-37.7 ± 1.7
MMP@$PEG_{150}OH$	-24.0 ± 1.1
MMP@$PEG_{2000}OH$	-22.4 ± 1.9

dipolar interaction or the formation of protein corona on the particle surface, which in the case of PEGylated particles is reduced due to the steric repulsion and anti-fouling ability.

Evaluation of toxicity of bare and functionalized magnetic microparticles

First, the intrinsic toxicity of the particles after a 24 h incubation with glioblastoma cells without the application of an external magnetic field was evaluated by two different tests: the WST-1 assay, which measures the cellular metabolic activity and the LDH leakage assay, which evaluates the cell membrane integrity by determining the amount of LDH enzyme released into the culture medium. Toxicity was assessed for the six different types of particles with various concentrations from 3 mg L^{-1} up to 0.2 g L^{-1} (or even up to 1 g L^{-1} for MMP and MMP@SiO_2) (supporting info Fig. S1†). It was found that the concentration of particles has no significant effect on the toxicity. Therefore, as examples, Fig. 4 shows the metabolic activity and the LDH leakage of glioblastoma cells 24 h after incubation with 50 mg L^{-1} (except otherwise indicated) for all the tested particles. Both tests indicate very limited toxicity with metabolic activity above 90% and non-significant LDH leakage, except for the MMP@$PEG_{280}NH_2$ and MMP@$PEG_{280}COOH$. Indeed, it was reported that the charge of particles plays a significant role in their toxicity.[36] Generally speaking, the charged particles are more toxic than neutral ones.[31] It has been demonstrated that coating inorganic nanoparticles with PEG-NH_2 increases their intracellular accumulation,[37] and this may be because of the positive charge of these particles, which promotes a better interaction of the inorganic particle with the negatively-charged cell membrane. This would explain the slightly higher cytotoxicity of MMP@$PEG_{280}NH_2$, which could potentially result from adhesion to the cell membrane leading to intracellular accumulation. Although it is still modest, these particles with relatively higher toxicity have been discarded for the following *in vitro* magneto-mechanical experiments. Also, based on previous results obtained with the same magneto-mechanical treatment of cancer cells, but with different magnetic particles, the particle concentration was fixed at 50 mg L^{-1}.[3,4] At this concentration, the MMP do not induce any significant cell mortality. Still, it should be kept in mind that this does not necessarily imply that they do not affect the cells, since the activation of some cell signaling has already been reported at sub-lethal concentrations of iron oxide nanoparticles.[21]

Efficacy of the magneto-mechanical treatment to promote cell death *via* apoptosis

The effects of the magneto-mechanical treatment on the metabolic activity and membrane permeability, with respect to the duration and frequency of the applied magnetic field, are then investigated and reported in Fig. 5 and 6, respectively. The study was performed using four different types of particles for comparison, including bare MMP, MMP@SiO_2, MMP@C_6-$PEG_{150}OH$ and MMP@$PEG_{2000}OH$.

Metabolic activity *vs.* duration of the magneto-mechanical treatment. As shown in Fig. 5a, generally speaking, more important cell damages are observed with a longer treatment duration. Besides, the impact of the treatment duration on the metabolic activity depends strongly on the nature of the particles. The most significant cell damages are observed with bare MMP, with an average metabolic activity of 42% after only 1 min

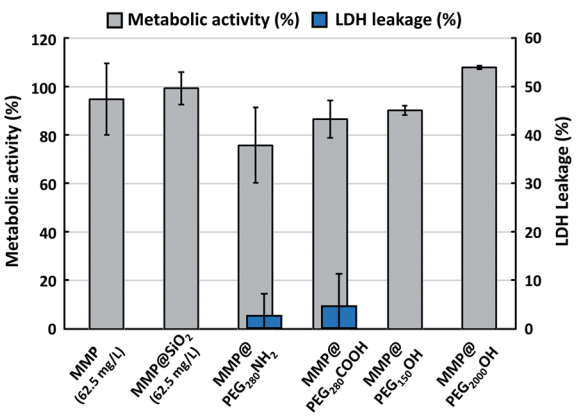

Fig. 4 Metabolic activity and LDH leakage of U87-MG cells after a 24 h incubation with 50 mg L^{-1} (unless otherwise indicated) of magnetic microparticles with different functionalization. The LDH leakage for samples with no reported result was not significant.

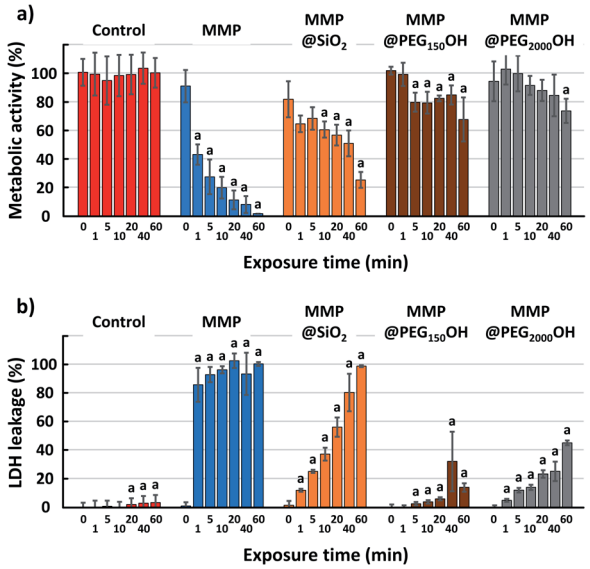

Fig. 5 (a) Metabolic activity and (b) LDH leakage of U87-MG cells 18 h after magneto-mechanical treatment at 20 Hz during 0, 1, 5, 10, 20, 40 or 60 min. One-way ANOVA for each group and then Student *t*-test. (a) $p < 0.05$ for Student *t*-test compared with the point at 0 min for the same group.

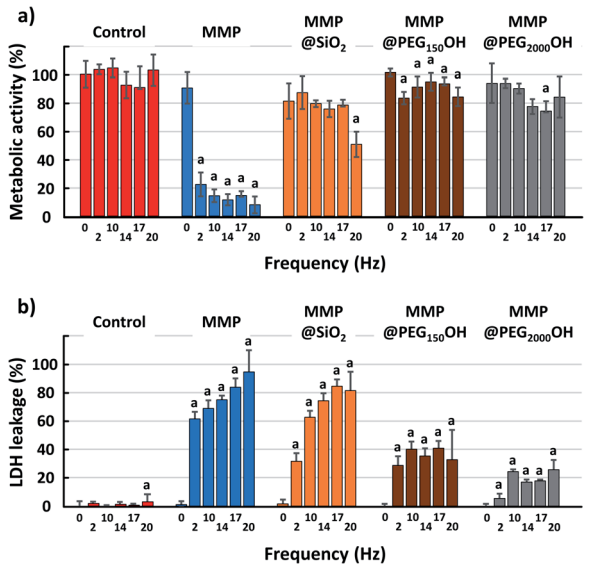

Fig. 6 (a) Metabolic activity and (b) LDH leakage of U87-MG cells 18 h after magneto-mechanical treatment during 40 min at 2, 10, 14, 17 or 20 Hz. One-way ANOVA for each group and then Student *t*-test. (a) $p < 0.05$ for Student *t*-test compared with the point at 0 Hz for the same group.

of magneto-mechanical treatment, followed by a regular decrease down to 1.4% after 60 min (Fig. 5a).

A large decrease in metabolic activity is also observed with MMP@SiO_2, but it is more gradual, with a significant decrease after 10 min and a value of 25% for metabolic activity after 60 min. On the other hand, the treatment with PEGylated MMP shows less pronounced decreases in metabolic activity with a value at 67% (MMP@$C_6PEG_{150}OH$) and 73% (MMP@$PEG_{2000}OH$) even after 60 min.

Cell membrane integrity *vs.* duration. As observed, the decrease in membrane integrity is massive and rapid with bare MPP (Fig. 5b). The average LDH leakage value is already at 86% after only one minute of treatment and the average value for the whole treatment duration is almost 96%. MMP@SiO_2 induce a different behavior with a LDH leakage value gradually increasing with treatment duration, from 12% after one minute up to nearly 100% after 60 min. In contrast, the PEGylated MMP show a much less pronounced effect on the membrane integrity, with a value for LDH leakage that increases steadily over time up to 14% (MMP@$C_6PEG_{150}OH$) and 45% (MMP@$PEG_{2000}OH$), respectively. These results show the importance of the MMP surface modification on their biomechanical action. In particular, PEGylation of MMP provides steric hindrance due to hydration of the PEG chains on the surface of the MMP. As anticipated, this stabilizes the MMP suspension, limiting their structuration as large agglomerates (supporting info Fig. S2†), which would be more damaging to cell membranes. Moreover, PEGylation would weaken the interactions between MMP and cell plasma membrane, as this steric hindrance introduces a gap between the MMP and the cell membrane. This in turn reduces the mechanical force applied to the membrane during the magnetic treatment, the latter causing membrane breakage leading to the release of LDH. Lastly, the MMP PEGylation, by changing the overall surface properties of the MMP, would lead to a different biomolecular corona coating the MMP. The biomolecular corona is defined as the pool of biomolecules that get adsorbed on the surface of a particle, thereby defining its "biological identity".[38] While it was thought that PEGylation would impair the biomolecular corona formation, recent studies rather showed that a biomolecular corona still forms on the surface of PEGylated particles, but that its composition differs from that of the biomolecular corona forming on bare particles.[39] This biomolecular corona plays a crucial role in the particle interaction with the cell membrane and consequently can modulate the efficacy of the magneto-mechanical treatment. This mitigation of the plasma membrane damaging potential *via* PEGylation of MMP is as efficient with PEG_{150} as with PEG_{2000}, showing that the steric hindrance provided by short PEG chains is sufficient to mitigate the cell damaging effect induced by the magneto-mechanical treatment.

Metabolic activity and cell membrane integrity *vs.* frequency. The frequency of the applied magnetic field is another important physical parameter of the magneto-mechanical treatment. For optimization purpose, its effect on metabolic activity and membrane integrity was also evaluated, at a fixed treatment duration of 40 minutes. As shown in Fig. 6a, the impact of the frequency on the metabolic activity of the cells is not very pronounced since the change that is recorded for all the tested particles is small. It appears, nevertheless, that the LDH leakage (Fig. 6b) is more dependent on this parameter, at least for the MMP and MMP@SiO_2 particles, with an increase in membrane damage from 61% to 94% for the MMP and from 31% to 81% for the MMP@SiO_2 when the frequency increases from 2 to

20 Hz. Moreover, at 2 Hz the LDH release is more intense when cells are treated with MMP@$PEG_{150}OH$, compared to MMP@$PEG_{2000}OH$. This suggests that, at this low frequency, the steric hindrance provided by the long $PEG_{2000}OH$ chains more efficiently mitigates the cell membrane damaging potential of the magneto-mechanical treatment, compared to the short $PEG_{150}OH$ chains.

Such discrepancy between the results of LDH and WST-1 assay are unexpected. Both assays are used classically as markers of cell viability, and it is generally accepted that cells with damaged membranes are not viable anymore. Consequently, cells showing intense LDH release would also show decreased metabolic activity *via* the WST-1 assay, while the opposite is not necessarily true (cells can show temporary reduced metabolic activity but remain viable, with no release of LDH). It suggests that cells could show transient membrane breakage due to the magneto-mechanical treatment, with no impact on their metabolism, and could stay alive.

Evaluation of the ratio of apoptotic cells

The previous results show that the MMP and MMP@SiO_2 seem to be the most effective in triggering cell death. Nevertheless, a closer look at the induced apoptotic response from the cells indicates that the picture is different in these two cases. For this, we choose to compare the change in the total number of cells in each culture well, and the change in the number of apoptotic cells, after 40 min magneto-mechanical treatment using different frequencies (Fig. 7).

As already observed when analyzing the evolution of cell metabolic activity and LDH leakage, application of the magneto-mechanical treatment to cells exposed to MMPs leads to the death of 90% of the cells, whatever the frequency of the applied magnetic field. Cell death is less intense when the cells are exposed to MMP@SiO_2, compared to bare MMP. Moreover, MMP PEGylation greatly reduces cell death, which is negligible when a 2 Hz magnetic field is applied on cells exposed to MMP@$PEG_{150}OH$ and MMP@$PEG_{2000}OH$ (Fig. 7a). Focusing on this condition, while most of the cells remain viable when treated with MMP@$PEG_{150}OH$ and MMP@$PEG_{2000}OH$, 13% and 11% of them, respectively, are apoptotic after application of the 2 Hz magneto-mechanical treatment (Fig. 7b). This level of apoptotic cells is comparable to what is generally observed upon magneto-mechanical treatments using more complex particles produced by a top-down approach.[4] This shows that the MMP used here, obtained from the simple processing of easily accessible material, and surface modified using classical techniques, are a promising alternative to those complex particles for future magneto-mechanical treatments.

Cell interaction with the magnetic microparticles

To delve into the mechanisms of the observed effects, the next question is whether the magnetic microparticles are simply adsorbed on the surface of cells, or whether they are internalized inside the cells. If adsorbed on the cell membrane, the induction of apoptosis could result from opening of mechano-receptors of the plasma membrane, leading to the influx of some ions such as calcium inside the cells, which would trigger apoptosis. Transmission electron microscopic observation of cells exposed to MMP, MMP@$PEG_{150}OH$ or MMP@$PEG_{2000}OH$ submitted to 2 Hz magneto-mechanical treatment shows that whatever their surface modification, magnetic microparticles both get adsorbed on the cell plasma membrane (*e.g.*, in Fig. 8C, *) and internalized inside cells (Fig. 8, arrows). This cellular adsorption and internalization shows that even negatively charged particles coated with long PEG chains can interact with negatively charged cell membranes. After the magneto-mechanical treatment, evidence of cell death is observed (Fig. 8D shows a dead cell, where organelles have been released in the extracellular compartment and are interacting with MMP@$PEG_{2000}OH$, surrounded by two live cells – upper and lower third of the image – with intact nucleus and mitochondria). Magnetic microparticles concentrate in the region of the fragmented dead cell; this may be due to release of intracellular components that locally modify the chemical characteristics of the milieu, triggering the particle agglomeration and/or interaction with dead cell fragments.

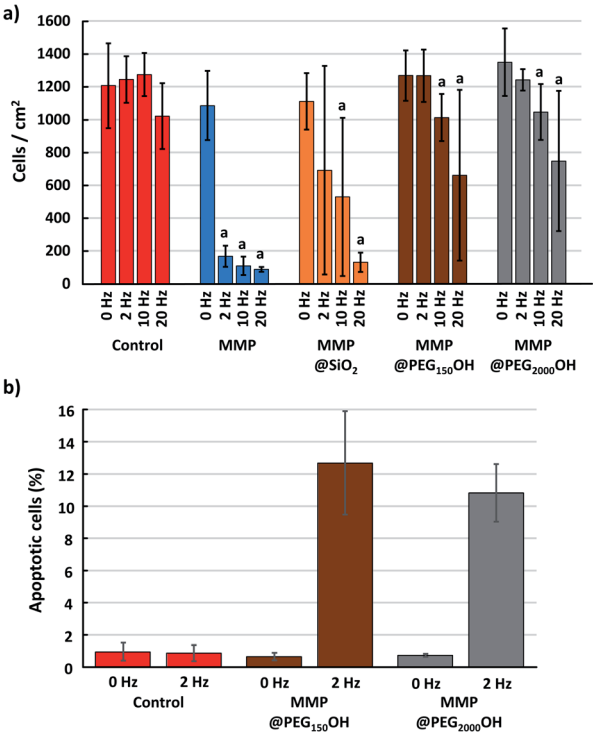

Fig. 7 (a) Number of cells per mm^2 measured 5 h after magneto-mechanical treatment during 40 min at 0, 2, 10 or 20 Hz. One-way ANOVA for each group and then Student *t*-test. (a) $p < 0.05$ for Student *t*-test compared with the point at 0 Hz for the same group. (b) Ratio of apoptotic cells relative to the number of cells per mm^2, for 0 Hz and 2 Hz.

Materials and methods

Materials

Magnetite powder (iron (II, III) oxide, Fe_3O_4, particle size <5 μm), tetraethyl orthosilicate (TEOS), (3-aminopropyl)

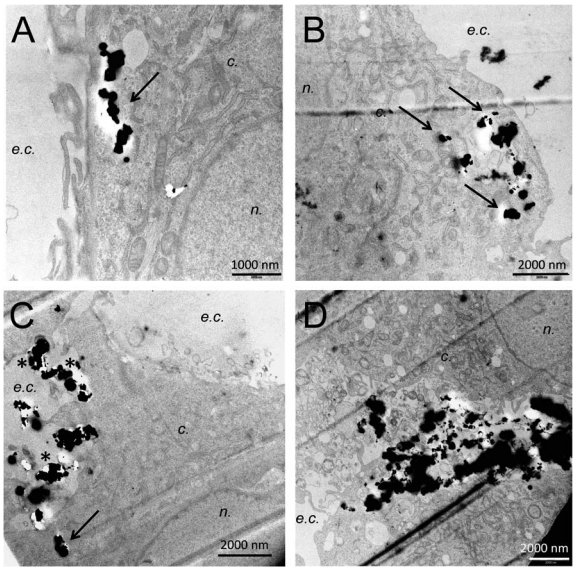

Fig. 8 Microparticles interaction with cell membrane and accumulation into the cell cytoplasm. Cells are exposed to 50 μg mL^{-1} of MMP (A and B), MMP@$PEG_{2000}OH$ (C and D) and submitted to a magneto-mechanical treatment at 2 Hz for 40 min (D); n.: nucleus, c.: cytoplasm, e.c.: extracellular compartment.

triethoxysilane (APTES), LDH and WST-1 kits were all purchased from Sigma-Aldrich. DMEM + Glutamax, succinimidyl 3-(2-pyridyldithio)propionate (SPDP), Hoechst 33342 and CellEvent Caspase-3/7 Green Detection Reagent were purchased from Thermo Fisher. PEGs (HS-PEG-X), including HS-C_6PEG_{150}-OH, HS-$C_{11}PEG_{280}$-NH_2, and HS-$C_{11}PEG_{280}$-OCH_2COOH were purchased from Prochimia Surfaces. The PEG HS-PEG_{2000}-OH was purchased from Creative PEGWorks. Glioblastoma cells U87-MG were purchased from ATCC.

Solvents (ethanol, isopropanol, and dimethyl sulfoxide (DMSO)), ammonium hydroxide solution (28% NH_3 in H_2O), phosphate buffered saline tablet (PBS, pH 7.4) were all supplied by Sigma-Aldrich. MilliQ ultrapure water (18.2 MΩ cm) was used in all experiments.

Particle fabrication by ball milling

0.5 g of magnetite powder was added to the 50 mL zirconia-coated grinding jars with 15 mL of isopropanol and 10 zirconia grinding balls, with 10 mm diameter. The planetary ball milling (Retsch-PM100) was performed for 1, 2, 4 or 12 h at 600 rpm with a 10 s pause every 10 min and with a change of the rotation direction. The obtained magnetite microparticles were washed twice with isopropanol by attracting the particles in the bottom of a tube with a magnet followed by supernatant removal. MMP were then dried, weighted and dispersed in isopropanol at 30 g L^{-1}.

Particle functionalization

The functionalization path is illustrated in Fig. 3 and detailed below.

Fe_3O_4@SiO_2. In the first step, MMP were coated with the silica shell following a modified Stöber process.[40,41] 2 mg of MMP was dispersed in ethanol at a concentration of 70 mg L^{-1} and 580 μL of ultrapure water, 1.3 mL of NH_3 at 28% and 1.7 mL of TEOS were added. The suspension was maintained at 40 °C for 2 h while agitating. The obtained Fe_3O_4@SiO_2 particles were sorted with a magnet and washed three times with ultrapure water. Fe_3O_4@SiO_2 were then re-dispersed in ultrapure water and stored at 4 °C.

Fe_3O_4@SiO_2@APTES. In the second step, the silica shell was functionalized by silanization using bifunctional organosilane APTES. For this, 2 mg of Fe_3O_4@SiO_2 was dispersed at 70 mg L^{-1} in a 1 : 1 mixture of ethanol and ultrapure water and 2% v/v of APTES was added.[42] The suspension was maintained at 50 °C for 24 h while agitating. The obtained Fe_3O_4@SiO_2@-APTES particles were carefully washed with ethanol and then with ultrapure water before being dispersed in PBS at 1 g L^{-1} and stored at 4 °C.

Fe_3O_4@SiO_2@APTES@SPDP@PEG-X. In the third step, PEG ligands were anchored onto the functionalized magnetic particles with the help of SPDP, a short-chain crosslinker for amine-to-sulfhydryl conjugation *via* NHS-ester and pyridyldithiol reactive groups that form cleavable disulfide bonds. For this, Fe_3O_4@SiO_2@APTES particles were dispersed in PBS at 65 mg L^{-1} and a solution of SPDP at 10 mM in DMSO was added (5.7×10^{-3} mol of SPDP per g of particles). The suspension was maintained at 25 °C for 1 h while agitating. The obtained Fe_3O_4@SiO_2@APTES@SPDP particles were thoroughly washed and dispersed in PBS at 3.5 g L^{-1}. Then, 1.4×10^{-4} mol of HS-PEG-X per g of particle were added from a solution at 10 mM in PBS. The suspension was maintained at 25 °C for 1 h while agitating. Afterwards, the suspension was thoroughly washed and dispersed in PBS at 4.7 g L^{-1}. 1.4×10^{-3} mol of 2-mercaptoethanol per g of particle were added from a solution at 20 mM in PBS and the suspension was kept in the same reaction conditions as with HS-PEG-X to block SPDP in excess. The obtained PEGylated particles Fe_3O_4@SiO_2@APTES@SPDP@PEG-X were washed, dispersed at 1 g L^{-1} in PBS and stored at 4 °C. In this study, four types of PEGylated particles Fe_3O_4@SiO_2@-APTES@SPDP@PEG-X were prepared using HS-PEG-X, including HS-$(CH_2)_6$-PEG_{150}-OH; HS-$(CH_2)_{11}$-PEG_{280}-NH_2; HS-$(CH_2)_{11}$-PEG_{280}-OCH_2COOH and HS-PEG_{2000}-OH.

Particle characterization

Scanning electron microscopy (SEM). MMP were dispersed at 0.3 g L^{-1} in ultrapure water and 2 μL of this suspension was deposited on a silicon wafer and let to dry. Then, the particles were observed using SEM and images were analyzed using the ImageJ software (National Institutes of Health, Bethesda) to measure their size. As the particles are not spherical, the measured parameters were the Feret and minimal Feret (Min-Feret) diameters (maximum and minimum distance between two parallel straight lines tangent to the particle). The Mean Feret and Mean MinFeret diameters associated to each synthesis were calculated by fitting their distribution with a lognormal law using Origin software (Northampton MA 01060

USA). The values of Feret diameter and MinFeret diameter for a given milling duration are averaged from 4 different sets of synthesis.

X-ray diffraction spectra (XRD). XRD were recorded with an X'Pert PANalytical system, with a Cu source (1.540598 Å). The Rietveld analysis of the recorded data was carried out using the HighScore Plus 3.0.5 analysis software.

Vibrating-sample magnetometer (VSM). For magnetization measurement, particles in solution were deposited on 5 mm × 5 mm silicon wafer and allowed to dry. The mass of particles was 1.66 mg. Hysteresis loop was recorded at room temperature with a Microsense EV vibrating sample magnetometer in magnetic fields up to 1 T.

Zeta potential. Zeta potential was measured with Univette in a LitesizerTM 500 (Anton Paar, Austria) on a suspension of particles at 0.16 g L^{-1} in PBS. The mean zeta potential was calculated from 500 measurements for each type of particle at 25 °C.

Cell culture

U87-MG glioblastoma cells were cultured in DMEM Glutamax medium supplemented with 10% of fetal bovine serum, 100 μM of streptomycin, and 100 units per mL of penicillin. They were maintained at 37 °C in a 5% CO_2-humidified atmosphere and passaged twice a week using 0.05% Trypsin-EDTA.

Toxicity assays

For cytotoxicity assays, cells were seeded in 96 well plates at a density of 50 000 cells per well in 100 μL of culture medium. 24 h after cell seeding, MMP were washed and dispersed in the culture medium at concentrations ranging from 3 mg L^{-1} to 1 g L^{-1} and 100 μL of each MMP suspension was applied to cells (6 wells per condition, $n = 6$). 0.1% Triton-X-100 was used as positive control. After 24 h of exposure, cell viability was assessed using LDH and WST-1 assays.

For the LDH leakage assay, 50 μL of the supernatant of each well was transferred to a clean 96 well plate. LDH assay substrate, cofactor and dye were mixed as recommended by the supplier, added to each well and incubated at room temperature in the dark for 5 min. The reaction was stopped by the introduction of 10 μL of 1 N HCl per well. The absorbance (Abs) was recorded at 490 nm with subtraction of the baseline signal at 690 nm. The percentage of LDH leakage was calculated as:

$$\%\ \text{LDH leakage} = \frac{(\text{Abs} - \text{mean}(\text{Abs}_{\text{healthy cells}}))}{(\text{mean}(\text{Abs}_{\text{Triton}}) - \text{mean}(\text{Abs}_{\text{healthy cells}}))} \times 100$$

For the WST-1 assay, after the sampling exposure medium for the LDH assay, the remaining supernatant was replaced by a 10% WST-1 solution prepared in cell culture medium and incubated for 1 h at 37 °C. Interference of nanoparticles with the readout of cytotoxicity assays has been largely described in the literature. To avoid such bias, the MMP were allowed to settle down at the bottom of the plate and 50 μL of the supernatant was transferred to a clean 96 well plate. The ability of metabolically-active cells to cleave WST-1 to formazan was evaluated *via* absorbance measurement at 450 nm and subtraction of the baseline signal at 650 nm. The percentage of viability was calculated as:

$$\%\ \text{Viability} = \frac{(\text{Abs} - \text{mean}(\text{Abs}_{\text{Triton}}))}{(\text{mean}(\text{Abs}_{\text{healthy cells}}) - \text{mean}(\text{Abs}_{\text{Triton}}))} \times 100$$

Magneto-mechanical treatment

Cells were seeded in 8 well LABTEK with 50 000 cells per well in 200 μL of culture medium and incubated for 24 h at 37 °C in a 5% CO_2-humidified atmosphere. MMP were washed and dispersed in the culture medium at 50 mg L^{-1} and 200 μL of this MMP suspension was applied to cells. After 4 h of incubation, the cells were placed inside a rotating Halbach cylinder, with a magnetic field of 0.6 T at its center. In one set of experiments, cells were treated with a RMF at 20 Hz for a duration of 1, 5, 10, 20, 40 and 60 min, respectively. In another set of experiments, cells were treated with the RMF for a fixed duration of 40 min with varied frequency of 2, 10, 14, 17 and 20 Hz, respectively.

LDH and WST-1 tests were performed 18 h after treatment as previously described.

Viabilities and LDH leakage were compared with the ones of cells treated with the same conditions of RMF but without the presence of magnetic particles. Cells exposed to Triton at 0.1% were used as positive control.

Evaluation of the efficacy of the magneto-mechanical treatment

The efficacy of the magneto-mechanical treatment was evaluated by measuring both the cell viability and the proportion of apoptotic cells after application of the magnetic field to the MMP. The viability was assessed *via* LDH leakage and WST-1 assays, 18 h after the magneto-mechanical treatment, using 0.1% Triton as positive control as described in the toxicity test section. The proportion of apoptotic cells was quantified *via* fluorescence microscopy observation after staining with the CellEvent Caspase 3/7 assay kit (Invitrogen) and 0.3 mg L^{-1} of Hoechst 33342, 5 h after the mechano-magnetic treatment. After 30 min of incubation at 37 °C, cells were observed by fluorescence microscopy. The ImageJ software (National Institutes of Health, Bethesda) was then used to count cells for determining the total number of cells (*i.e.* the number of nuclei, stained blue by Hoechst 33342) and the number of apoptotic cells (stained green by the CellEvent marker).

Transmission electron microscopy (TEM)

For TEM imaging, after exposure to MMP and magneto-mechanical treatment, cells were rinsed with PBS, fixed in 2% glutaraldehyde prepared in cacodylate buffer then post-fixed using 1% osmium tetroxide. They were then dehydrated through a graded series of ethanol and embedded in Epon resin. Ultra-thin sections were cut and stained with 1% uranyl

acetate. Sections were observed on a JEOL 1200EX TEM operating at 80 kV (Grenoble Institut des Neurosciences, Grenoble, France).

Conclusions

We prepared anisotropic magnetite microparticles by liquid-phase ball milling of a magnetite powder, with magnetic properties such that a magnetic field induces mechanical vibration. After coating the particles with silica (MMP@SiO_2), different PEGylated molecules were grafted to the surface thanks to a 3-step functionalization (MMP@$C_6PEG_{150}OH$, MMP@$PEG_{2000}OH$, MMP@$C_{11}PEG_{280}NH_2$, MMP@$C_{11}PEG_{280}COOH$).

The particles showed very low *in vitro* intrinsic cytotoxicity on human glioblastoma U87-MG cells, while significant cell death was observed under RMF. To optimize the magneto-mechanical treatment efficacy, the metabolic activity and the LDH leakage were measured while varying the RMF frequency (2–20 Hz) and exposure time (1–60 min). Our results indicate that (1) the magneto-mechanical treatment with bare MMP induced a rapid decrease in cell viability whereas the effect was slower with PEGylated particles; (2) the number of apoptotic cells after magneto-mechanical treatment was higher with PEGylated particles; (3) a lower RMF frequency (down to 2 Hz) favored apoptosis. These results highlight a difference in the cell death mechanism according to the type of particle used – the rapid cell death observed with MMP favoring necrosis, while PEGylated particles rather induce apoptosis.

Conflicts of interest

There are no conflicts of interest to declare.

Acknowledgements

This work has received support from the European Union through the H2020 ERA-Net EuroNanoMed II project Nanoviber. The authors would like to thank Christine Saint-Pierre for the zeta potential measurement.

References

1 S. M. Dadfar, K. Roemhild, N. I. Drude, S. von Stillfried, R. Knüchel, F. Kiessling and T. Lammers, *Adv. Drug Delivery Rev.*, 2019, **138**, 302–325.
2 D. H. Kim, E. A. Rozhkova, I. V. Ulasov, S. D. Bader, T. Rajh, M. S. Lesniak and V. Novosad, *Nat. Mater.*, 2010, **9**, 165–171.
3 S. Leulmi, X. Chauchet, M. Morcrette, G. Ortiz, H. Joisten, P. Sabon, T. Livache, Y. Hou, M. Carrière, S. Lequien and B. Dieny, *Nanoscale*, 2015, **7**, 15904–15914.
4 C. Naud, C. Thébault, M. Carrière, Y. Hou, R. Morel, F. Berger, B. Diény and H. Joisten, *Nanoscale Adv.*, 2020, **2**, 3632–3655.
5 F. Broders-Bondon, T. H. N. Ho-Bouldoires, M. E. Fernandez-Sanchez and E. Farge, *J. Cell Biol.*, 2018, **217**, 1571–1587.
6 Q. A. Pankhurst, N. T. K. Thanh, S. K. Jones and J. Dobson, *J. Phys. D: Appl. Phys.*, 2009, **42**, 224001.
7 V. S. Markin and F. Sachs, *Phys. Biol.*, 2004, **1**, 110–124.
8 D. Gonzalez-Rodriguez, L. Guillou, F. Cornat, J. Lafaurie-Janvore, A. Babataheri, E. de Langre, A. I. Barakat and J. Husson, *Biophys. J.*, 2016, **111**, 2711–2721.
9 Y. I. Golovin, S. L. Gribanovsky, D. Y. Golovin, N. L. Klyachko, A. G. Majouga, A. M. Master, M. Sokolsky and A. V. Kabanov, *J. Controlled Release*, 2015, **219**, 43–60.
10 S. Leulmi, H. Joisten, T. Dietsch, C. Iss, M. Morcrette, S. Auffret, P. Sabon and B. Dieny, *Appl. Phys. Lett.*, 2013, **103**, 132412.
11 M. Goiriena-Goikoetxea, D. Muñoz, I. Orue, M. L. Fernández-Gubieda, J. Bokor, A. Muela and A. García-Arribas, *Appl. Phys. Rev.*, 2020, **7**, 011306.
12 A. R. Muxworthy, D. J. Dunlop and W. Williams, *J. Geophys. Res.: Solid Earth*, 2003, **108**, 2281.
13 T. P. Almeida, A. R. Muxworthy, A. Kovács, W. Williams, L. Nagy, P. Ó. Conbhuí, C. Frandsen, R. Supakulopas and R. E. Dunin-Borkowski, *Geophys. Res. Lett.*, 2016, **43**, 8426–8434.
14 H. Joisten, T. Courcier, P. Balint, P. Sabon, J. Faure-Vincent, S. Auffret and B. Dieny, *Appl. Phys. Lett.*, 2010, **97**, 253112.
15 S. Wilhelm, A. J. Tavares, Q. Dai, S. Ohta, J. Audet, H. F. Dvorak and W. C. W. Chan, *Nat. Rev. Mater.*, 2016, **1**, 16014.
16 M. Torrice, *ACS Cent. Sci.*, 2016, **2**, 434–437.
17 D. Rosenblum, N. Joshi, W. Tao, J. M. Karp and D. Peer, *Nat. Commun.*, 2018, **9**, 1410.
18 A. Frtús, B. Smolková, M. Uzhytchak, M. Lunova, M. Jirsa, Š. Kubinová, A. Dejneka and O. Lunova, *J. Controlled Release*, 2020, **328**, 59–77.
19 B. Kharazian, N. L. Hadipour and M. R. Ejtehadi, *Int. J. Biochem. Cell Biol.*, 2016, **75**, 162–174.
20 F. Yuan, M. Dellian, D. Fukumura, M. Leunig, D. A. Berk, V. P. Torchilin and R. K. Jain, *Cancer Res.*, 1995, **55**, 3752–3756.
21 M. Uzhytchak, B. Smolková, M. Lunova, M. Jirsa, A. Frtús, Š. Kubinová, A. Dejneka and O. Lunov, *Cells*, 2020, **9**, 1015.
22 E. Zhang, M. F. Kircher, X. M. Koch, L. Eliasson, S. N. Goldberg and E. Renstro, *ACS Nano*, 2014, **8**, 3192–3201.
23 O. Lunov, M. Uzhytchak, B. Smolková, M. Lunova, M. Jirsa, N. M. Dempsey, A. L. Dias, M. Bonfim, M. Hof, P. Jurkiewicz, Y. Petrenko, Š. Kubinová and A. Dejneka, *Cancers*, 2019, **11**, 1873.
24 P. Clerc, P. Jeanjean, N. Hallali, M. Gougeon, B. Pipy, J. Carrey, D. Fourmy and V. Gigoux, *J. Controlled Release*, 2018, **270**, 120–134.
25 A. M. Master, P. N. Williams, N. Pothayee, N. Pothayee, R. Zhang, H. M. Vishwasrao, Y. I. Golovin, J. S. Riffle, M. Sokolsky and A. V. Kabanov, *Sci. Rep.*, 2016, **6**, 33560.
26 J. Rejman, V. Oberle, I. S. Zuhorn and D. Hoekstra, *Biochem. J.*, 2004, **377**, 159–169.
27 M. Contreras, R. Sougrat, A. Zaher, T. Ravasi and J. Kosel, *Int. J. Nanomed.*, 2015, **10**, 2141–2153.
28 M. M. Song, W. J. Song, H. Bi, J. Wang, W. L. Wua, J. Sun and M. Yu, *Biomaterials*, 2010, **31**, 1509–1517.

29 I. Papageorgiou, C. Brown, R. Schins, S. Singh, R. Newson, S. Davis, J. Fisher, E. Ingham and C. P. Case, *Biomaterials*, 2007, **28**, 2946–2958.
30 K. Turcheniuk, A. V. Tarasevych, V. P. Kukhar, R. Boukherroub and S. Szunerits, *Nanoscale*, 2013, **5**, 10729–10752.
31 E. Fröhlich, *Int. J. Nanomed.*, 2012, **7**, 5577–5591.
32 S. Gates-Rector and T. Blanton, *Powder Diffr.*, 2019, **34**, 352–360.
33 F. Bosi, U. Halenius and H. Skogby, *Am. Mineral.*, 2009, **94**, 181–189.
34 B. D. Cullity and C. D. Graham, *Introduction to Magnetic Materials*, 2nd edn, 2008.
35 Q. Li, C. W. Kartikowati, S. Horie, T. Ogi, T. Iwaki and K. Okuyama, *Sci. Rep.*, 2017, **7**, 9894.
36 N. M. Schaeublin, L. K. Braydich-Stolle, A. M. Schrand, J. M. Miller, J. Hutchison, J. J. Schlager and S. M. Hussain, *Nanoscale*, 2011, **3**, 410–420.
37 A. Kolate, D. Baradia, S. Patil, I. Vhora, G. Kore and A. Misra, *J. Controlled Release*, 2014, **192**, 67–81.
38 A. Aliyandi, I. S. Zuhorn and A. Salvati, *Front. Bioeng. Biotechnol.*, 2020, **8**, 599454.
39 S. Schöttler, G. Becker, S. Winzen, T. Steinbach, K. Mohr, K. Landfester, V. Mailänder and F. R. Wurm, *Nat. Nanotechnol.*, 2016, **11**, 372–377.
40 W. Stober, A. Fink and E. Bohn, *J. Colloid Interface Sci.*, 1968, **26**, 62–69.
41 P. Riani, M. A. Lucchini, S. Thea, M. Alloisio, G. Bertoni and F. Canepa, *Inorg. Chem.*, 2014, **53**, 9166–9173.
42 S. Villa, P. Riani, F. Locardi and F. Canepa, *Materials*, 2016, **9**, 826.